A&A 502, 817–832 (2009)
DOI: 10.1051/0004-6361/200810615

Astronomy & Astrophysics

The photometric evolution of dissolving star clusters⋆,⋆⋆

II. Realistic models. Colours and M/L ratios

P. Anders[1], H. J. G. L. M. Lamers[1], and H. Baumgardt[2]

[1] Sterrenkundig Instituut, Universiteit Utrecht, PO Box 80000, 3508 TA Utrecht, The Netherlands
e-mail: P.Anders@uu.nl
[2] Argelander Institut für Astronomie, Universität Bonn, Auf dem Hügel 71, 53121 Bonn, Germany

Received 15 July 2008 / Accepted 14 May 2009

ABSTRACT

Context. Evolutionary synthesis models are the primary means of constructing spectrophotometric models of stellar populations, and deriving physical parameters from observations compared with these models. One of the basic assumptions of evolutionary synthesis models has been the time-independence of the stellar mass function, apart from the successive removal of high-mass stars by stellar evolution. However, dynamical simulations of star clusters in tidal fields have demonstrated that the mass function can be changed by the preferential removal of low-mass stars from clusters.
Aims. We combine the results of dynamical simulations of star clusters in tidal fields with our evolutionary synthesis code GALEV. We extend the models to consider the total cluster disruption time as additional parameter.
Methods. Following up on our earlier work, which was based on simplifying assumptions, we reanalyse the mass-function evolution found in N-body simulations of star clusters in tidal fields, parametrise it as a function of age and total disruption time of the cluster, and use this parametrisation to compute GALEV models as a function of age, metallicity, and total cluster disruption time.
Results. We study the impact of cluster dissolution on colours (which generally become redder) and magnitudes (which become fainter) of star clusters, their mass-to-light ratios (which can deviate by a factor of ∼2–4 from predictions of standard models without cluster dissolution), and quantify the effect of the altered integrated photometry on cluster age determination. In most cases, clusters appear to be older than they are, where the age difference can range from 20% to 200%. By comparing our model results with observed M/L ratios for old compact objects in the mass range $10^{4.5}$–10^{8} $M_{\odot}$, we find a strong discrepancy for objects more massive than 10^{7} $M_{\odot}$, such that observed M/L ratios are higher than predicted by our models. This could be caused either by differences in the underlying stellar mass function or be an indication of the presence of dark matter in these objects. Less massive objects are well described by the models.

Key words. Galaxy: globular clusters: general – Galaxy: open clusters and associations: general – galaxies: star clusters – methods: data analysis

1. Introduction

Since the pioneering work of Tinsley (Tinsley 1968; Tinsley & Gunn 1976; Tinsley 1980), evolutionary synthesis modelling has become the method-of-choice for predicting spectrophotometric properties of stellar populations. Popular models include STARBURST99 (Leitherer et al. 1999), GALAXEV (Bruzual & Charlot 2003), GALEV (Anders & Fritze-v. Alvensleben 2003; Bicker et al. 2004; Kotulla et al. 2009), PEGASE (Fioc & Rocca-Volmerange 1997), and the Maraston models (Maraston 2005), all giving predictions for single-age populations, so-called "Simple Stellar Populations" (SSPs). In addition, GALAXEV, PEGASE, and GALEV provide models for populations with arbitrarily extended star formation histories (SFH, like galaxies), while STARBURST99 only allows for an extended constant SFH. Comparing predictions from these models with observations allows us to derive basic physical parameters of the studied system (e.g., among many others, Bicker et al. 2002; Kassin et al. 2003; Anders et al. 2004b; de Grijs et al. 2004; Kundu et al. 2005; de Grijs & Anders 2006; Smith et al. 2007).

While the specific input physics, such as the choice of stellar isochrones and spectral libraries, the inclusion of gaseous emission, and their implementation varies among the models, some basic techniques and limitations are inherent to all of them. Specifically, a spectrum is assigned to each star along the isochrone, weighted according to a chosen stellar initial mass function (IMF) and all of these spectra are then integrated along the isochrone (and over the SFH, if applicable), to predict the integrated properties of the stellar population at a given age. For all currently available models, the stellar mass function (MF) is time-independently fixed at its initial value, the IMF.

Cluster disruption[1] has become a well-studied phenomenon. It can be observed both in the earliest phases of a cluster's life (the so-called "infant mortality" caused by the removal

⋆ The models for a range of total cluster disruption times and metallicities are available online, at http://www.phys.uu.nl/~anders/data/SSP_varMF/ and http://data.galev.org

⋆⋆ The data will also be made available in electronic form at the CDS via anonymous ftp to cdsarc.u-strasbg.fr (130.79.128.5) or via http://cdsweb.u-strasbg.fr/cgi-bin/qcat?J/A+A/502/817

[1] With *disruption* we comprise all kinds of different cluster mass loss and destruction *events* (e.g., single disruptive encounters with giant molecular clouds, infant mortality, final cluster "death"). *Dissolution* stands for any gradual destruction *process*, e.g., mass lost due to stellar evolution, tidal dissolution, or multiple weak encounters with giant molecular clouds.

of gas left over from the cluster formation process by stellar winds and/or the first supernovae, see e.g. Lada & Lada 2003; Bastian & Goodwin 2006) and for old clusters (e.g., the prominent tidal tails of the Milky Way globular cluster Palomar 5, Odenkirchen et al. 2003). Age and mass distributions of an entire star cluster *system* can be used to determine the typical disruption time of clusters of a given mass in this cluster system (Boutloukos & Lamers 2003; Lamers et al. 2005b; Gieles et al. 2005). This cluster disruption time is predominantly determined by the external tidal field that the cluster is experiencing (see Lamers et al. 2005b), the local density of giant molecular clouds (Gieles et al. 2006), and the occurrence of spiral arm passages (Gieles et al. 2007). In addition, the cluster loses mass due to stellar evolution. While in the case of "infant mortality", the cluster is likely (almost) completely disrupted (although a bound core might remain, see e.g., Bastian & Goodwin 2006, for "infant weight loss"), *cluster dissolution* in a smooth external tidal field is a more gradual process accompanied by perpetual dynamical readjustment within the cluster. The latter is characterised by a mass-dependent probability to remove a star from a cluster: because of energy equipartition, massive stars tend to sink towards the cluster centre, while low-mass stars are driven outwards where they are more easily removed by the surrounding tidal field (Henon 1969; Spitzer & Shull 1975; Giersz & Heggie 1997). The resulting radial dependence of the mean stellar mass inside a cluster is called "mass segregation". Mass segregation established by the very star formation process itself is referred to as "primordial mass segregation" (for observational evidence of "primordial mass segregation", see e.g. Gouliermis et al. 2004; Chen et al. 2007).

Baumgardt & Makino (2003, hereafter: BM03) performed the first (and, so far, most extensive) quantitative large-scale study of how the stellar MF inside a star cluster changes because of dynamical cluster evolution in a tidal field. They confirmed earlier findings of a preferential loss of low-mass stars and derived a formula describing the change in MF slope for low-mass stars. However, their derived formula (formula (13) in BM03) applies only to stars with masses $\leq 0.5\ M_{\odot}$, while the effect is pronounced also for higher-mass stars (see BM03 Fig. 7), which dominate the flux emerging from the cluster (for ages shorter than a Hubble time). BM03 performed their simulations for clusters that are not primordially mass-segregated. In Baumgardt et al. (2008), they also studied the dissolution of initially mass-segregated clusters (with a simplified initial setup that differs from the BM03 simulations, hence we cannot combine these sets of simulations), finding an even stronger MF evolution than BM03. Marks et al. (2008) studied the evolution of the stellar MF inside star clusters during the gas removal/"infant weight loss" phase, and found it to also preferentially remove low-mass stars, leading to a flattening or even turning-over of the MF. This effect is most pronounced for initially mass-segregated clusters, and would be amplified by the later dynamical cluster evolution, as presented in BM03. Although their results cannot be straightforwardly combined with the BM03 results (due to differences in model setups), both studies suggest even further enhancement of the effects studied in this paper.

In Lamers et al. (2006), we constructed simplified evolutionary synthesis models for solar metallicity, based on the GALEV models and the results from BM03. The main simplification concerned the description of the changing (logarithmic) MF, which we modelled with fixed slopes, but a time-dependent lower mass limit (i.e., assuming that only the lowest-mass stars are removed from the cluster, while higher-mass stars might only be removed by stellar evolution). We scaled our models to match the total mass in stars with $M < 2\ M_{\odot}$ with the BM03 simulations.

This approach was improved by Kruijssen & Lamers (2008) who incorporated the effects of stellar remnants and produced cluster models of different initial masses, different total disruption times and a range of metallicities. They showed that the presence of stellar remnants plays a dominant role in the mass evolution of the clusters and therefore also in the evolution of the mass-to-light ratio. They also found that metallicity affects the colour evolution of the clusters, not only by the difference in the colours of the stars, but also by influencing the cluster dynamics due to the sensitivity of stellar mass and remnant formation on metallicity. They determined colours and mass-to-light ratios for a range of metallicities. Kruijssen (2008) compared these predicted mass-to-light ratios with the observed ones for cluster samples in different galaxies (Milky Way, Cen A, M 31, and LMC) and found that the effects of mass segregation (and the associated preferential loss of low-mass stars) can explain the observed range much better than the range predicted by standard SSP models. Since the models of Kruijssen & Lamers (2008) are based on the simplified assumption that only the *lowest-mass stars* are removed from the cluster, they can be improved by models in which the mass function changes in a more physically realistic manner, i.e. the *slope* of the (logarithmic) mass function changes in a way derived from dynamical N-body simulations. This is the purpose of this paper.

We describe our input physics in Sect. 2. In particular, we reanalyse the data presented in BM03 to derive formulae parametrising the changing mass function (Sect. 2.3). In Sect. 3 we present our new evolutionary synthesis models, and discuss their implications for determinations of mass-to-light (M/L) ratios and cluster ages from observations. In Sect. 4, we present a comparison with previous models (Lamers et al. 2006; Kruijssen & Lamers 2008) and investigate the impact of model uncertainties (fit uncertainties, initial-final mass relations, and isochrones). We finish with our conclusions in Sect. 5.

2. Input physics

In this section we will summarise the input physics of the new star cluster models. This includes: the N-body simulations considered (Sect. 2.1), the definition and calculation of the cluster masses (Sect. 2.2), and the parametrisation of the changing mass function (Sect. 2.3).

2.1. N-body simulations by BM03

BM03 carried out a parameter study of the dynamical evolution of clusters dissolving in a tidal field. They studied clusters with a range of particle numbers (8 k–128 k, i.e., a range in cluster mass) on circular and elliptical orbits at different Galactocentric distances (i.e., strengths of the surrounding gravitational field). They accounted for mass lost due to stellar evolution (using fit formulae by Hurley et al. 2000), two-body relaxation, and the external tidal field.

They initialised their clusters with a universal Kroupa (2001) IMF, which is of the form:

$$\xi(m)\mathrm{d}m \sim \begin{cases} m^{-1.3}\mathrm{d}m & m < 0.5\ M_{\odot} \\ m^{-2.3}\mathrm{d}m & m \geq 0.5\ M_{\odot} \end{cases} \quad (1)$$

with masses in the range $0.1\ M_{\odot} \leq m \leq 15\ M_{\odot}$. This rather low upper mass limit was chosen to account for the uncertain

kick velocities of neutron stars (or equivalently, their ejection probability from the cluster, see BM03 for details).

The MFs provided by BM03 are of single stars, where dynamically created binaries are resolved in their components. They provide the MF for the entire cluster (i.e., for all stars within the tidal radius). This MF compares well with the MF around the half-mass radius of the cluster, as shown by BM03.

BM03 do *not* take into account primordial mass segregation and primordial binaries. However, primordial mass segregation is found to increase even further the changes in the MFs found by BM03 (see Baumgardt et al. 2008). Primordial binaries seem to have little impact on the stars *evaporating* slowly from a cluster (see Küpper et al. 2008), but enhance the number of stars violently *ejected* during strong binary interactions. However, the latter are still only a small fraction of the stars leaving the cluster, hence we expect little changes in our conclusions if simulations with primordial binaries are included in our studies.

BM03 do not include an intermediate-mass black hole (IMBH) in the cluster. Gill et al. (2008) found that the presence of an IMBH reduces mass segregation in the centre, which might also influence the mass loss from star clusters, although this has still not been shown. In addition, the existence of IMBHs in star clusters remains unclear (see e.g. Maccarone & Servillat 2008).

2.2. Total cluster disruption time and the total cluster mass

In a way similar to BM03, we identify the "total cluster disruption time" with the time when only 5% of the initial cluster mass remains bound. To avoid confusion, we specifically label this time $t_{95\%}$, i.e., the time when the cluster has lost 95% of its initial mass. However, we provide our models for ages up to the point where a cluster with an initial mass of $10^6\ M_\odot$ has lost all but $10^2\ M_\odot$ of its luminous mass (or to a maximum age of 16 Gyr, whichever occurs first). This termination age of the cluster models is ~20–26% longer than the cluster disruption time $t_{95\%}$ (for models with termination ages <16 Gyr, see Fig. 5, bottom panel).

As defined by Boutloukos & Lamers (2003) and Lamers et al. (2005b), we use $t_4 = t_{\rm dis}^{\rm total}(M = 10^4\ M_\odot)$, the total disruption time of a $10^4\ M_\odot$ star cluster, as a rough proxy for characterising the strength of the gravitational field surrounding a cluster: the stronger the field the faster the cluster will dissolve, and the shorter t_4. Using the implicit equation

$$t_{\rm dis}^{\rm total}(M_{\rm i}) = t_4 \cdot \left(\frac{M_{\rm i}}{10^4\ M_\odot}\right)^{\gamma} \cdot \left(\frac{\mu_{\rm ev}(t_{\rm dis}^{\rm total})}{\mu_{\rm ev}(t_4)}\right)^{\gamma} \quad (2)$$

for the total disruption time $t_{\rm dis}^{\rm total}$ (see Lamers et al. 2005a), t_4 can be translated into the total disruption time of clusters with arbitrary initial mass $M_{\rm i}$. For example, a gravitational field characterised by $t_4 = 1.3$ Gyr (the value found by Lamers et al. 2005b for the Solar Neighbourhood) leads to complete disruption of a cluster with $10^3\ M_\odot$ within approximately 300 Myr, while a $10^6\ M_\odot$ cluster would survive for 22.6 Gyr. $\mu_{\rm ev}(t)$ describes the fraction of the mass that the cluster would have at time t if stellar evolution was the only mass-loss mechanism, and $\gamma = 0.62$ (as determined from observations by Boutloukos & Lamers 2003; Lamers et al. 2005b, and in agreement with N-body simulations, see BM03 and Gieles & Baumgardt 2008).

The total cluster mass as a function of the fractional age $t/t_{95\%}$ is derived from Eq. (6) in Lamers et al. (2005a), who also show good agreement with the data from BM03:

$$M_{\rm tot}(t) = M_{\rm i} \cdot \left\{\mu_{\rm ev}(t)^{\gamma} - \frac{t}{t_{95\%}} \cdot \left[\mu_{\rm ev}(t_{95\%})^{\gamma} - 0.05^{\gamma}\right]\right\}^{1/\gamma} \quad (3)$$

where $M_{\rm i} = 10^6\ M_\odot$ is the initial cluster mass. The stellar evolution part of this equation was taken directly from the GALEV models used in the remainder of this work (for details see below). Since the total disruption time of clusters in a given environment (e.g. tidal field) depends on the initial cluster mass, Eq. (3) can also be used to calculate the initial cluster mass for an observed present-day total mass and adopted $t_{95\%}$.

The mass fraction in stellar remnants is taken from BM03 (their Eq. (16)):

$$f_{\rm rem}(t) = f_{\rm rem}^{\rm se}(t) + 0.18 \cdot \left(\frac{t}{t_{95\%}}\right)^2 + 0.16 \cdot \left(\frac{t}{t_{95\%}}\right)^3 \quad (4)$$

where $f_{\rm rem}^{\rm se}$ is the mass fraction in stellar remnants from stellar evolution only (i.e., without dynamical cluster evolution effects) taken from our GALEV models, and the other two terms describe the increase in the mass fraction of the remnants caused by the preferential loss of low-mass non-remnant stars.

The luminous mass is then

$$M_{\rm lum}(t) = M_{\rm tot}(t) \cdot (1 - f_{\rm rem}(t)). \quad (5)$$

2.3. Parametrising the time-dependence of the mass function

Throughout the paper, we consider the logarithm of the logarithmically binned mass function (MF). Hence, for a Salpeter (1955) IMF, the *power-law index* –2.35 becomes a *linear slope* of –1.35.

To parametrise the changes in the (logarithmic) mass function, we

- took the MF data from BM03
- divided these by the IMF (by doing so we remove the power law break at 0.5 $M_\odot$ in the Kroupa 2001 IMF)
- skipped the 2 highest not-empty mass bins (since those are affected and partially emptied by stellar evolution), and
- fitted the remainder with a piecewise power law, independently for every simulation and age.

We tried fitting slopes and break point simultaneously and found the results for the break point to scatter in the range 0.25–0.35 $M_\odot$. This scatter was found to be uncorrelated with any other quantity, confirming its random nature. Hence, we chose a double power-law with a break point fixed to be 0.3 $M_\odot$, and only fitted the slopes below and above this break point independently for every simulation and age. In Fig. 1, we show the slopes of the changing MF, relative to the slopes of the IMF (i.e., $\alpha(t) - \alpha(0)$). The points are derived by fitting the data from BM03, using the aforementioned scheme, and the median in bins of $\Delta(t/t_{95\%}) = 0.025$ was then taken. The error bars represent the 16% and 84% percentiles of individual data points in each bin, equivalent to 1σ ranges for a Gaussian distribution. These data are grouped according to their disruption time $t_{95\%}$: $t_{95\%} \le 3.5$ Gyr = filled orange diamonds, 3.5 Gyr $< t_{95\%} \le 6$ Gyr = open blue triangles, 6 Gyr $< t_{95\%} \le 10$ Gyr = filled green circles, and 10 Gyr $< t_{95\%}$ = open black squares. This fit formula, in conjunction with the Kroupa (2001) IMF, leads to a 3-component power-law MF with break points at 0.3 $M_\odot$ and 0.5 $M_\odot$ and time-dependent slopes.

The time evolution of the MF slopes can be expressed as

$$\begin{aligned}\alpha(t) = {} & \alpha_{\rm IMF}(0) \\ & + a_1 \cdot x + a_2 \cdot x^2 + a_3 \cdot x^3 + a_4 \cdot x^4 \\ & + b \cdot x \cdot t\end{aligned} \quad (6)$$

where "t" is the cluster age in Myr, while "x" $= t/t_{95\%}$ is the fractional cluster age in units of its total disruption time. The best-fit

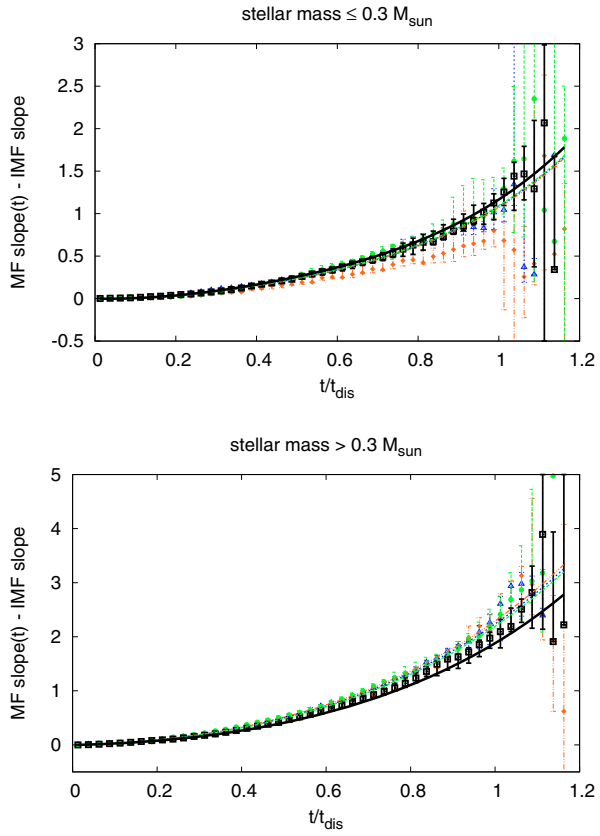

Fig. 1. Dependence of MF slopes (*top panel*: for stellar masses ≤0.3 $M_\odot$, *bottom panel*: for stellar masses >0.3 $M_\odot$) on the fractional age $t/t_{95\%}$. Symbols represent median slopes (and 16% and 84% percentiles uncertainty ranges) derived from individual data from BM03 runs, and binned in intervals of $\Delta(t/t_{95\%}) = 0.025$. The data are grouped according to their disruption times: $t_{95\%} \leq 3.5$ Gyr (filled orange diamonds), 3.5 Gyr $< t_{95\%} \leq 6$ Gyr (open blue triangles), 6 Gyr $< t_{95\%} \leq 10$ Gyr (filled green circles), 10 Gyr $< t_{95\%}$ (open black squares). Smooth lines represent the fit formula (6) for the respective age ranges: $t_{95\%}$ = 1 Gyr (orange dot-dot-dashed line), 5 Gyr (blue, dotted), 8 Gyr (green, dashed) and 30 Gyr (black, solid). Shown is the difference between the time-dependent slope of the MF and the slope of the IMF (i.e. $\alpha(t) - \alpha(0)$).

Table 1. The best-fit coefficients for Eq. (6). The middle column gives the coefficients for the low-mass end of the MF for masses ≤0.3 $M_\odot$. The right column gives the coefficients for masses >0.3 $M_\odot$.

Coefficient	$m \leq 0.3\ M_\odot$	$m > 0.3\ M_\odot$
a_1	–0.1345	0.08389
a_2	1.7986	1.9324
a_3	–1.8121	–0.4435
a_4	1.2181	0.734
b	3.215e-6	–1.4143e-5

The middle column gives the coefficients for the low-mass end of the MF for masses ≤0.3 $M_\odot$. The right column gives the coefficients for masses >0.3 $M_\odot$.

coefficients are provided in Table 1. These fit parameters have a very high formal accuracy, because of the large number of data points used in the fit. However, the spread of N-body models around our best fit is the dominant source of uncertainty (see below and Sect. 4.1). We therefore omit the formal fit uncertainties in Table 1.

In Fig. 1, we overplot our fit formulae for 4 disruption times $t_{95\%}$ (1 Gyr, 5 Gyr, 8 Gyr, and 30 Gyr), which are representative of the chosen grouping in disruption time.

We restrict the fitting to ages $\leq t_{95\%}$, since in many cases clusters with older ages do not contain enough stars to determine the MF slopes with reasonable accuracy. However, the general trends continue beyond $t_{95\%}$, following the fitted relation further on, allowing an extrapolation for ages $> t_{95\%}$ (see Fig. 1).

In addition, we take into account only simulations started with 32 k or more particles (these simulations have total disruption times in the range 2.3–25.5 Gyr), since many simulations with lower particle numbers show substantial uncertainties in the determined MF slopes.

We emphasize that considering all simulations with either 16 k or more particles or 64 k or more particles yield fitted slopes that deviate from the 32 k results by less than ±0.1 for ages of up to at least $1.3 \times t_{95\%}$. Considering also 8 k simulations or only the 128 k simulations yields larger deviations, due to the large run-to-run scatter and small amount of data/coverage of parameter space, respectively.

On average, the spread in the BM03 simulation results around the fitted relation Eq. (6) is of the order of 15%, as shown in Figs. 2 and 3. For ages $\lesssim 1/3 \times t_{95\%}$, these *relative* deviations are larger, however, the *absolute* deviations of the data from the fit formulae are small (of the order of Δslope = 0.02–0.03). The impact of this uncertainty is discussed further in Sect. 4.1.

Although the BM03 simulations are performed for a metallicity $Z = 0.001$ (using the fitting formulae from Hurley et al. 2000), we use Eq. (6) for all metallicities, assuming the metallicity to – at most – introduce second-order effects on the cluster dynamics. This is supported by Hurley et al. (2004), who found that metallicity effects largely cancel each other, resulting in a weak overall metallicity dependence of cluster dynamics (although details are metallicity-sensitive).

2.4. The GALEV models

The GALEV models are extensively described in Schulz et al. (2002), Anders & Fritze-v. Alvensleben (2003), and Bicker et al. (2004). We provide here only a brief summary of the relevant input physics used.

The GALEV models used in this work are based on isochrones from the Padova group, first presented in Bertelli et al. (1994), and subsequently updated to include the TP-AGB phase[2]. This update, although not documented in a refereed publication, was made publicly available approximately in 1999, and treats the TP-AGB phase as later described in Girardi et al. (2000). Since we concentrate mainly on the evolution of old stellar clusters, the Padova isochrones were chosen instead of the Geneva isochrones (Schaller et al. 1992). We want to emphasize (and stimulate discussion amongst the various groups of stellar evolution modellers) that the isochrone sets by Bertelli et al. (1994) and Schaller et al. (1992) (and associated papers) are the *only* available isochrones that cover stellar evolution (in a *consistent* way) until its final stages as well as a mass range up to ~120 $M_\odot$ required to correctly model ongoing star formation in galaxies. (For further discussion of this point see Sect. 4.3.) For consistency with the BM03 simulations we use a Kroupa (2001) IMF.

At each age, the time-dependent MF is evaluated using Eq. (6) for the appropriate total disruption time $t_{95\%}$. To each star from the isochrones we assign the appropriate spectrum from

[2] The models of the Padova group are available at their webpage: http://pleiadi.pd.astro.it/

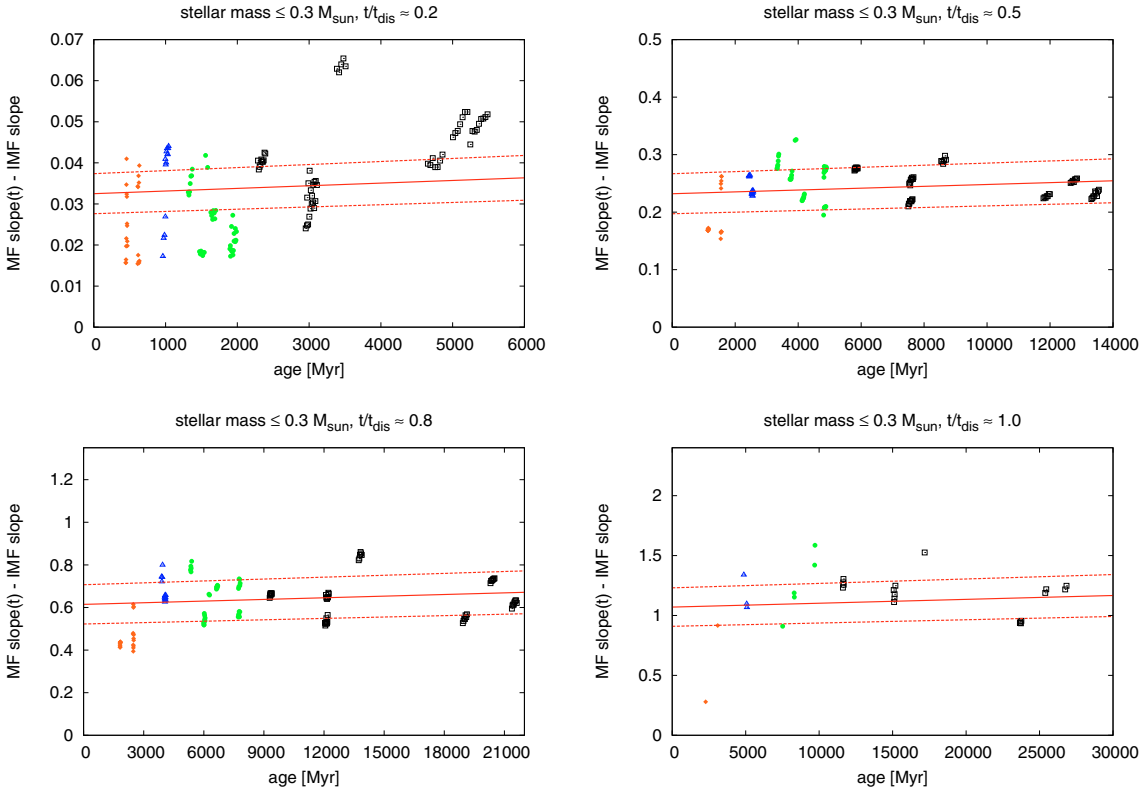

Fig. 2. Dependence of MF slope on the age (in Myr) of the cluster for stellar masses ≤0.3 $M_\odot$ and for 4 different fractional ages $t/t_{95\%}$: $t/t_{95\%}$ = 0.15–0.25 (*top left panel*), $t/t_{95\%}$ = 0.45–0.55 (*top right*), $t/t_{95\%}$ = 0.75–0.85 (*bottom left*), and $t/t_{95\%}$ = 0.95–1.05 (*bottom right*). In each panel, the solid line represents the fit formula (6) for the appropriate $t/t_{95\%}$, the dashed lines represent the median spread ranges (85% and 115% of fit line). Points are the same as Fig. 1. Please beware of the very different vertical axes. The y-axes are chosen to go from 0 to 2 × maximum fit value.

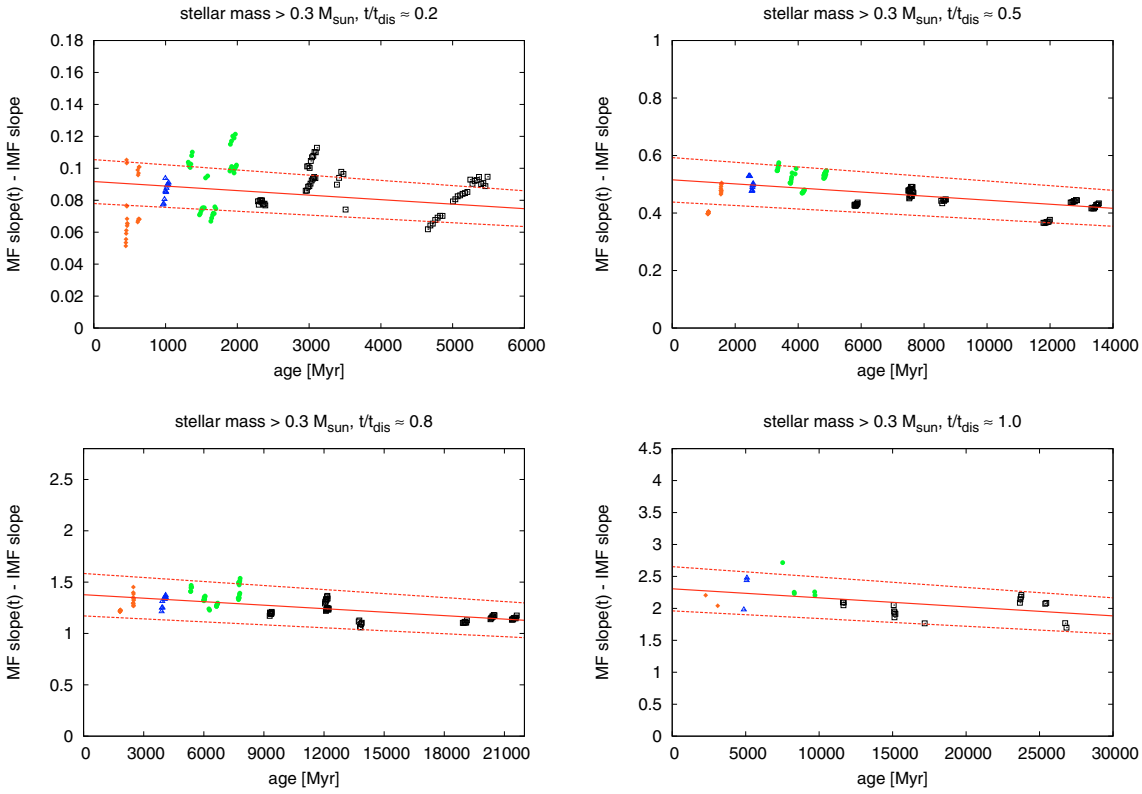

Fig. 3. Same as Fig. 2, but for stellar masses >0.3 $M_\odot$.

the BaSeL library (Lejeune et al. 1997, 1998) and a weight according to the time-dependent MF. The integrated spectra is then obtained by summing up the contributions from the individual stars. Here, we assume a well-populated MF, hence any stochastic effects caused by small number statistics, especially at the high-mass end of the MF, are neglected, and we model an *average* star cluster.

The treatment of stochastic effects is beyond the scope of this paper. Their impact was studied in depth by Cerviño and collaborators (see e.g., Cerviño & Mollá 2002; Cerviño & Luridiana 2004, 2006) and Fagiolini et al. (2007), who found these effects to be strongly age- and wavelength-dependent. The strongest impact was found for red passbands, which are dominated by a few red supergiants (young clusters) or very bright upper RGB and AGB stars (intermediate-age clusters). For non-dissolving clusters, the impact was found to become smaller for older ages. However, the decreasing number of stars with age in our dissolving cluster models probably cancels this reduction. We therefore discourage users against applying our models to single clusters. The models represent *average* star clusters of the given parameters, hence should be applied to a complete star cluster system.

More generally, small number statistics is the likely origin of the scatter seen in Figs. 2 and 3. However, as we use 19 BM03 models with a variety of parameters (i.e. total masses and dissolution times) to model the dissolution we can describe the *average* cluster dissolution. The impact of the spread seen in Figs. 2 and 3 will be discussed in more detail in Sect. 4.1.

Because of computational restrictions, we calculated individual models only for MF slopes with 2 decimal places. If at any given age the MF slopes were identical to within these 2 decimal places with the MF slopes of a previously computed model, we reused this older model. Due to this finite step-size, some cluster colours exhibit small jumps for successive ages of the order of ∼0.001 mag (up to 0.004 mag in the most extreme cases).

The spectrophotometry is normalised to a luminous cluster mass as described in Sect. 2.2.

We calculate models for $t_{95\%}$

- in the range of 100–900 Myr: in 50 Myr steps
- in the range of 1–16 Gyr: in 500 Myr steps
- for $t_{95\%}$ = 18, 20, 25, 30, 40, 60, 100, 150 and 200 Gyr

and for metallicities (limited by the metallicities provided by the Padova isochrones)

- $Z = 0.0004 \leftrightarrow$ [Fe/H] = – 1.7;
- $Z = 0.004 \leftrightarrow$ [Fe/H] = – 0.7;
- $Z = 0.008 \leftrightarrow$ [Fe/H] = – 0.4;
- $Z = 0.02 = Z_\odot \leftrightarrow$ [Fe/H] = 0.0;
- $Z = 0.05 \leftrightarrow$ [Fe/H] = + 0.4.

For $t_{95\%} \gtrsim 200$ Gyr, within a Hubble time the MF slopes deviate from the universal Kroupa (2001) IMF by less than 0.005. For conditions similar to the Solar Neighbourhood, i.e., $t_4 = 1.3$ Gyr as determined by Lamers et al. (2005b), the range in total disruption times corresponds to a cluster mass range 160–3.4×10^7 $M_\odot$ (i.e., a 160 $M_\odot$ cluster needs 100 Myr to become totally disrupted, a 10^4 $M_\odot$ cluster needs 1.3 Gyr, and a 3.4×10^7 $M_\odot$ cluster needs 200 Gyr). For the SMC, with $t_4 =\sim 10$ Gyr, the range in total disruption times would correspond to a cluster mass range of 6–1.25×10^6 $M_\odot$.

We provide the user with integrated cluster magnitudes in a variety of passbands and cluster masses (total mass, luminous mass, and mass in stellar remnants) for each of the models. Integrated spectra are available upon request[3].

3. Results and implications

We present our new models for solar metallicity (unless stated otherwise) and discuss their implications[4]. We would like to emphasize that the absolute values of our models (and therefore also the results and implications discussed in this section) depend on our choice of isochrones and other input physics. In Sect. 4 we discuss some of these uncertainties. The main results, the systematic differences induced by the preferential mass loss, are hardly changed.

3.1. Photometry

The photometry for the new models is shown in Fig. 4. The colours are shown as differences between the new models with a changing MF and the standard models with a fixed (initial) MF. For illustrative purposes, in the bottom left panel the absolute values of the *V*-*I* colour are presented. The *V*-band magnitude evolution (bottom right panel) is given in absolute magnitudes for a 10^6 $M_\odot$ cluster.

The *V*-band magnitude evolution shows the stellar evolution fading line as bright limit to the new models, which they follow for young ages, when the effect of mass loss is not yet pronounced. After ∼10% of their respective total disruption times, the new models have already evolved 0.1 mag away from the fiducial fading line, due to the loss of stars. At ∼80% (±10%, depending on the model) of their respective total disruption times, the new models are 1 mag fainter than standard models predict, due to the loss of stars.

Except for the very earliest stages of cluster evolution (the first few Myr), the flux in passbands redder than the *V* band is dominated by stars initially more massive than the main contributors to the flux in bluer passbands. This is caused by the flux in the red passbands being dominated by red (super)giants, which are more luminous than the stars at the low-mass end of the main sequence (MS), even after taking into account the higher number of low-mass MS stars provided by the IMF. For a changing MF due to dynamical evolution, the contribution from low-mass MS stars is even further reduced.

The dominant source of flux contribution in passbands including and bluewards of the *V* band is a strong function of time: at early stages, the flux is dominated by mid-MS stars (the evolution through the Hertzsprung gap is too fast to contribute significantly). As the cluster ages, the MS turn-off (MSTO) shifts successively redwards through the filters, ever increasing its contribution to the band's flux. However, the relative contribution of mid-MS stars and MSTO stars is also strongly dependent on the MF, and hence is dependent on the total disruption time of our models.

Since the selective mass loss preferentially removes the least massive stars from the cluster (and therefore its integrated photometry), it causes the cluster to become generally redder than the standard models without cluster dissolution (i.e., with infinite total cluster disruption time). The MF evolution and the

[3] The data are made publicly available at our webpages http://www.phys.uu.nl/~anders/data/SSP_varMF and http://data.galev.org. They will be made available via CDS as well.

[4] The data are made publicly available at our webpages http://www.phys.uu.nl/~anders/data/SSP_varMF and http://data.galev.org. They will be made available via CDS as well.

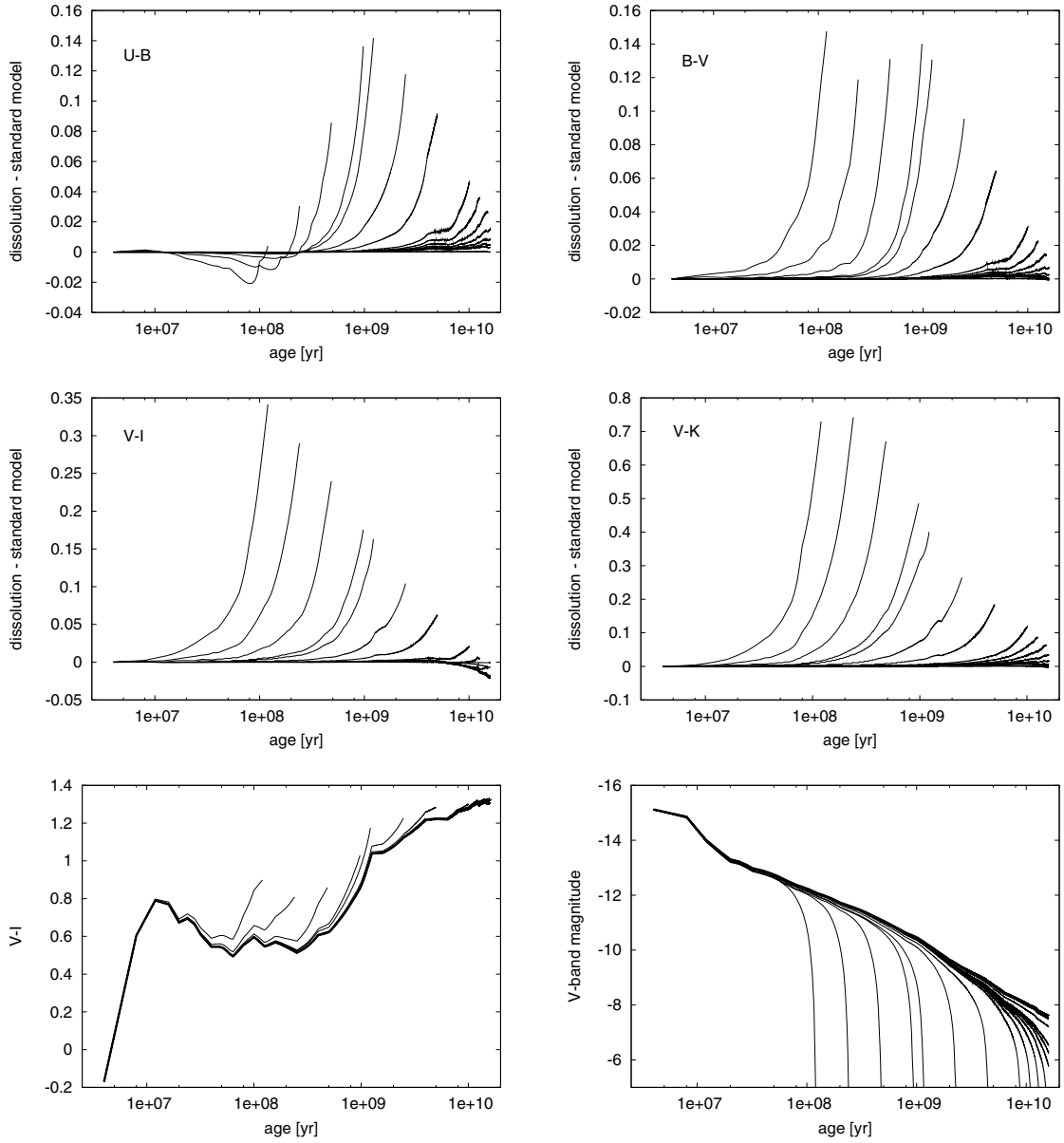

Fig. 4. Solar metallicity models with the changing mass function treatment, following Eq. (6) with $t_{95\%}$ in the range 100 Myr–100 Gyr (for clarity only models at 100, 200, 400, 800 Myr and 1, 2, 4, 8, 10, 12, 14, 16, 18, 20, 40, 100 Gyr are shown), going *from left to right*, respectively. *Upper left panel*: $U-B$ colour, *top right*: $B-V$, *middle left*: $V-I$, *middle right*: $V-K$. For these colours, the differences between the new models and the standard models are displayed. *Bottom left*: the absolute values for $V-I$, *bottom right*: V-band magnitude evolution of a 10^6 $M_\odot$ cluster. Thick lines represent the standard models.

resulting reddening speeds up while the cluster approaches its final disruption, leading to the steep colour evolutions towards the end of a cluster's lifetime, as seen in Fig. 4.

Two exceptions are noted:

- the colour $U-B$ (and similar colours) becomes bluer than the standard models for total disruption times shorter than ∼1 Gyr. At these ages, the B band is dominated entirely by mid-MS stars, while bluer bands contain contributions from the higher MS stars and the MSTO stars. Since the mid-MS is depopulated more significantly than the upper MS and MSTO because of the dynamical cluster evolution, the colours become bluer. For longer total disruption times the mid-MS is not sufficiently depopulated to be affected by this effect until the B band becomes sensitive to the contributions of the MSTO stars. Redder passbands are unaffected by this effect because they are more sensitive to the contributions of bright red (super-)giants.
- for colours such as $V-R$ and $V-I$ and ages $\gtrsim$6 Gyr, the models become slightly bluer than the standard models for total disruption times $\gtrsim$10 Gyr. This is probably caused by the strong depopulation of the lower MS (and the standard IMF containing a high number of stars at low masses), which leaves an imprint even though a single lower-MS star is 3–4 mag fainter than an RGB/AGB star of similar temperature. Redder passbands are unaffected because the magnitude difference between lower-MS stars and RGB/AGB stars increases with increasing wavelength and decreasing temperature, and the total contribution from MS stars decreases.

For long total disruption times, the maximum colour deviation in our models for dissolving clusters from the standard models

decreases with increasing total disruption time. This is caused by several effects:

- for such old ages, the MF covers only a narrow mass range in both cases;
- the integrated cluster flux is dominated by the upper-RGB/AGB stars, since they are significantly brighter than the MSTO region (the magnitude difference between upper-RGB/AGB and MSTO increases with time), resulting in an even narrower "effectively visible MF" range;
- the temperature range that these stars cover is significantly smaller than at younger ages, resulting in a lower sensitivity of the colours to the exact distributions of stars along the isochrone.

However, the changes in mass/absolute magnitude (see Fig. 4, bottom right panel) and M/L ratio (see next section) are significant in all cases.

The increasing maximum colour deviation in our dissolving clusters models from the standard models for blue passbands and increasing total disruption times $\lesssim$1 Gyr originates from the redward shifting of the MSTO through the filters.

The low-mass stars preferentially removed in the course of cluster dissolution have mass-to-light (M/L) ratios that are higher than the M/L ratio of the average cluster star. On the other hand, as shown by BM03, the fraction of (non-luminous) stellar remnants in dissolving clusters is enhanced in relation to the standard models. These effects partially cancel each other and lead to the time-dependent M/L ratios shown in Fig. 5, which demonstrates that for each total disruption time the M/L ratio of our dissolving cluster models is systematically lower than a standard model would suggest for the majority of a cluster's total disruption time. During the final stages of cluster dissolution (up to ~16% of a cluster's total disruption time), the M/L ratio can become enhanced compared to the standard models (see Fig. 5, bottom panel), because of the increasing fraction of stellar remnants inside the cluster.

In Fig. 6, we present the dependence of the V-band M/L ratio on the present cluster mass. The top panel shows how this relation evolves with cluster age at a field strength (i.e., location in a galaxy as characterised by t_4, the total disruption time of a $10^4\,M_\odot$ cluster described in Sect. 2.2) that is representative of the Solar Neighbourhood, as found by Lamers et al. (2005a). As the clusters evolve, the M/L ratio generally increases due to stellar evolution. In addition, the lowest-mass clusters eventually disrupt (and drop out of this plot). The highest-mass clusters lose mass, but still have M/L ratios close to the canonical value for stellar evolution. Intermediate-mass clusters are affected most by the changing mass function, which reduces their M/L ratio significantly compared to the canonical value. A few cases of *enhanced* M/L ratios can be seen for clusters close to final disruption (at the low-mass end of the curves).

In Fig. 6, (top panel) we overplotted data of young (ages < 1 Gyr) LMC and SMC clusters by McLaughlin & van der Marel (2005) (labelled "MM05", for details of this dataset see following subsection) and Larsen and collaborators (labelled "Larsen") in 4 spiral and irregular galaxies, (see Larsen & Richtler 2004 and Larsen et al. 2004). Out of the 13 clusters in these samples, 8 have M/L ratios consistent with our models for their respective ages (within their 1σ uncertainty ranges). The remaining 5 clusters all have too high M/L ratios for their respective ages. Two clusters are very young (~10 Myr), and hence could be out of equilibrium during their gas expulsion and readjustment phase, and their velocity dispersions might not trace their dynamical masses (see Goodwin & Bastian 2006). The deviations from the model predictions of the remaining clusters might be indications of errors in the models, or could be signs that the age determination is uncertain or the velocity dispersions are seriously affected by the orbital motions of binaries or other

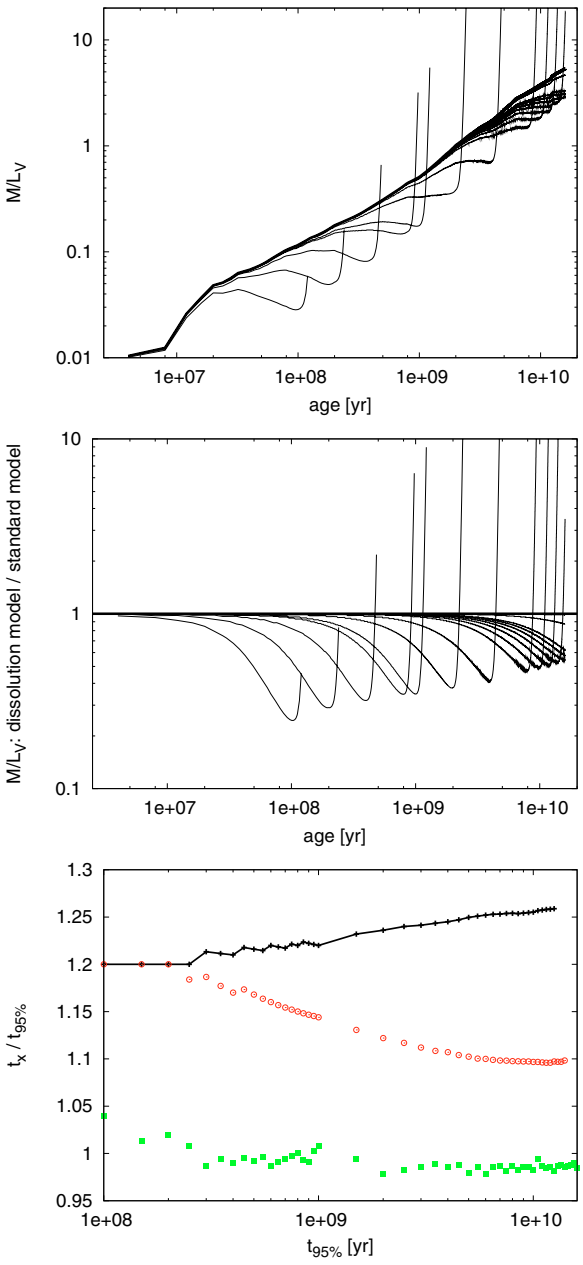

Fig. 5. Same models as Fig. 4, but M/L ratios. *Upper panel*: time evolution of V-band M/L ratio for the new models. *Middle panel*: ratio of new model's V-band M/L ratio and V-band M/L ratio from standard models. The non-dissolving/standard model is shown as thick line. *Bottom panel*: characteristic times of the models as function of total disruption time: black crosses and line = age at which the cluster contains only 100 $M_\odot$ luminous matter (i.e. termination age of model); red open circles = age at which the M/L ratio evolution crosses the standard model; green filled squares = age at which the M/L ratio of the dissolving cluster models is minimal w.r.t. the standard models (i.e. the dip seen in the *middle panel*). Only models for which the respective age is smaller than the maximum model age of 16 Gyr are shown.

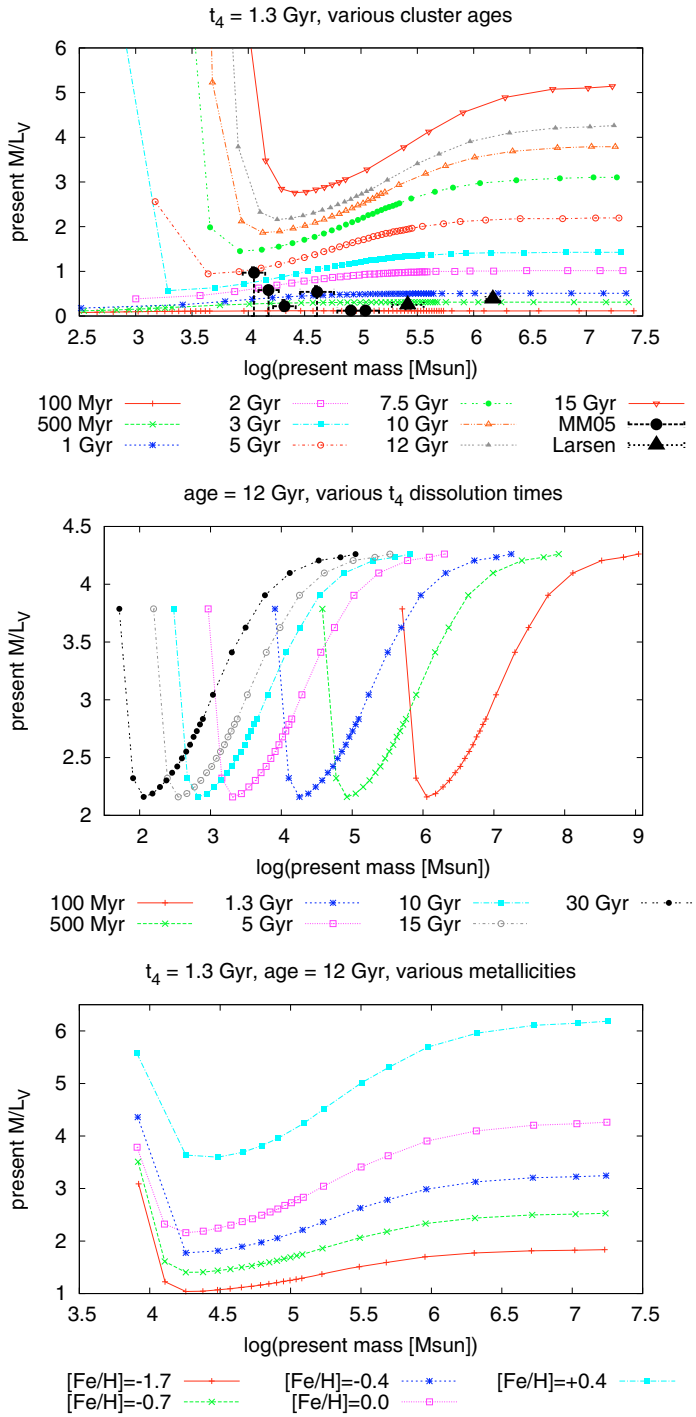

Fig. 6. *Top panel*: time evolution of V-band M/L ratio (for solar metallicity) as a function of present-day cluster mass for a fixed local gravitational field strength characteristic for the Solar Neighbourhood (i.e. t_4 = 1.3 Gyr, see Lamers et al. 2005a). *Middle panel*: V-band M/L ratio (for solar metallicity) as a function of present-day cluster mass for a range of local gravitational field strengths for clusters observed at an age of 12 Gyr. *Bottom panel*: V-band M/L ratio as a function of present-day cluster mass for a range in metallicity for clusters observed at an age of 12 Gyr and experiencing a typical disruption time t_4 = 1.3 Gyr. In the top panel, observations from McLaughlin & van der Marel (2005) (MM05) and from Larsen & Richtler 2004; Larsen et al. 2004 are overplotted, for young clusters with ages < 1 Gyr.

systematic observational effects, such as macroturbulence in the stellar atmospheres or instrumental resolution.

The middle panel shows the M/L ratio in the V band as a function of the present-day mass of 12 Gyr old clusters, for a range of gravitational field strengths (i.e., typical disruption times t_4). Within each line, the cluster's total disruption time ranges from 10 Gyr (low mass end; clusters with shorter total disruption times have been disrupted by an age of 12 Gyr) to 200 Gyr (upper end of available total disruption time range). For example, a cluster located at a position in a galaxy characterised by a field strength at t_4 = 1.3 Gyr (i.e., the blue line, corresponding to the environment in the Solar Neighbourhood), observed now (i.e., at an age of 12 Gyr) with a mass = 10^6 $M_\odot$, is expected to have a M/L_V of ~4, while a cluster with a mass = 10^4 $M_\odot$ has a model M/L_V of ~2.3.

The bottom panel shows the impact of metallicity on the M/L ratios: with increasing metallicity, the M/L_V ratio based on stellar evolution increases. Therefore, all curves reach higher M/L_V ratios at higher metallicities, while the shape of the curves is largely unaffected. At the high-mass end, all curves become constant at their respective values determined by stellar evolution alone. By comparing the top and bottom panels of Fig. 6, both for our new models and the non-dissolving standard models, the well-known age-metallicity degeneracy is apparent (see e.g., Worthey 1994).

Since the GALEV code (as most other evolutionary synthesis codes) is incapable of directly dealing with stochastic effects (especially the stochastic effects inherent to the selective mass loss caused by dissolution), we employ the following estimation scheme:

- we assume, that the majority of stochasticity originates in evolved stars (mainly RGB, and AGB stars);
- as a function of age, we determine the ratio of evolved to unevolved stars (i.e., MS stars);
- from this ratio, we determine the total number of evolved stars for clusters of different masses, and the stochastic scatter (i.e., the square root of the total number of evolved stars);
- we determine average properties of the evolved stars (mean effective temperature, mean log (g), and mean luminosity);
- We multiply the stochastic scatter by the spectrum of the mean evolved star, and either add or subtract this from our standard spectrum.

From this approach, we estimate the effect of IMF stochasticity on the M/L ratios to be roughly: 15, 5, and 1.5% uncertainty for clusters of total mass 10^4, 10^5, and 10^6 $M_\odot$, respectively. This test was done only for the standard, not depopulated IMF. The effects will be smaller for the depopulated MF, as for the same total mass, the number of giant stars will be higher.

Our results show features similar to those presented by Kruijssen & Lamers (2008) and applied by Kruijssen (2008). However, systematic differences are present, inherent to the underlying assumptions, and discussed in Sect. 4.4.

3.2. Mass-to-light ratios

3.2.1. Comparison with observations

We compare our new models with old globular clusters (and other old massive stellar systems) in the Milky Way and other galaxies. This is a first step in validating our models.

Figure 7 compares our new models with observational data from McLaughlin & van der Marel (2005) and Mieske et al. (2008). The colour coding of the data refers to their metallicity:

- blue = [Fe/H] < –1.2 = "MP" (metal-poor);

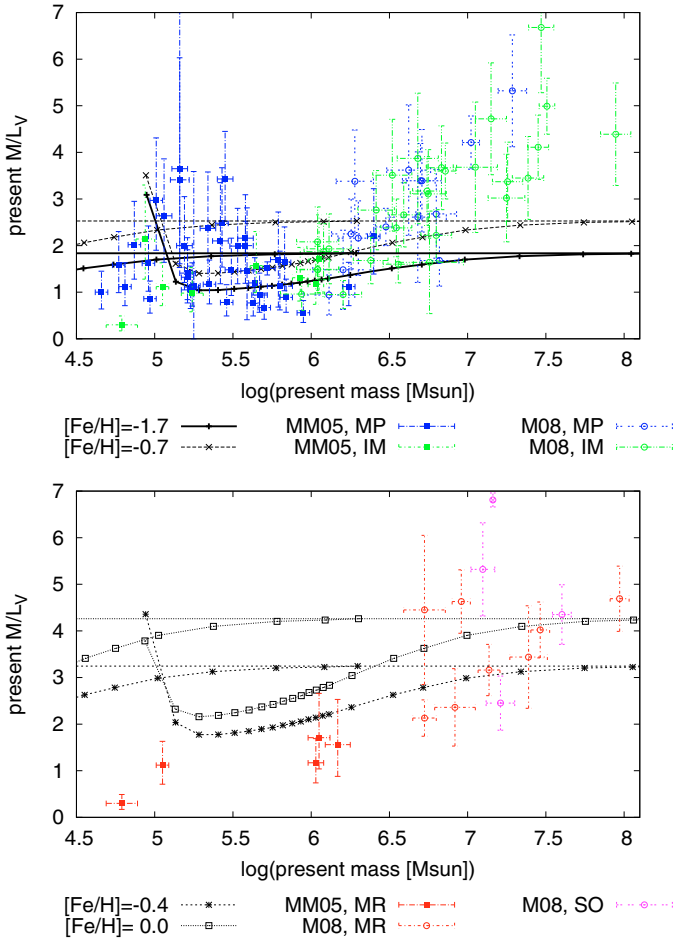

Fig. 7. Observations of old (~12 Gyr) objects from McLaughlin & van der Marel (2005, MM05) and Mieske et al. (2008, M 08). *Top panel*: objects with [Fe/H] < –0.55. Bottom panel: objects with [Fe/H] ≥ –0.55. Overplotted are our model V-band M/L ratio as a function of present-day cluster mass for the appropriate metallicities, at 12 Gyr and for typical disruption times t_4 = 300 Myr (*lower/right* branches for each metallicity) and t_4 = 5 Gyr (upper/left branches). Horizontal lines at the canonical values of M/L from stellar evolution are also shown. They represent the limit of infinite disruption times. These models are intended to illustrate the range covered by our models, and the inconsistency of most obsverations with models of infinite disruption time.

- green = –1.2 ≤ [Fe/H] < –0.55 = "IM" (intermediate metallicity);
- red = –0.55 ≤ [Fe/H] < –0.2 = "MR" (metal-rich);
- magenta = –0.2 ≤ [Fe/H] = "SO" (around solar).

These ranges were chosen to be consistent with the metallicities of both the Padova isochrones, and our models. Three objects from the cited samples are not shown in these plots due their high M/L ratios: LMC-NGC2257 and MW-NGC 6535 from McLaughlin & van der Marel (2005), which have M/L ratios of the order of 8–10 with error bars of the order of 4–5, and the Virgo cluster object S999 (with M/L = 10.2, from the Mieske et al. 2008 sample), which might have a genuinely high M/L ratio.

Overplotted are 2 sets of models for metallicities in the range from [Fe/H]= –1.7 to 0.0 (as is appropriate for the shown observational data), for cluster ages of 12 Gyr, and local tidal field strengths at t_4 = 5 Gyr (upper/left branches of models of a given metallicity, representative for halo clusters) and t_4 = 300 Myr (lower/right branches, representative for strong dissolution). The main point of the comparison is to illustrate the range of M/L$_V$ values that can be described by our models. As can be seen in Fig. 7, most Galactic GCs have M/L values compatible with our predictions and many, especially low-mass ones are below those of the standard isochrones. The estimated uncertainties of a few per cent, as estimated above for clusters in this mass range, are insufficient to bring the observations into agreement with the standard predictions from stellar evolution alone. We take this as clear evidence for cluster evolution/dissolution and that our evolving cluster models are a clear improvement over standard isochrone fitting for GCs.

Data for the Milky Way and the LMC are taken from McLaughlin & van der Marel (2005), the most extensive homogenised compilation of star cluster M/L ratios (which provides also other star cluster properties) for these galaxies. The majority of the data for the Milky Way was originally published by Pryor & Meylan (1993). Pryor & Meylan (1993) found a weak correlation between M/L ratio and mass, consistent with our models, but with large scatter and uncertainties (on average about 50–60%) and M/L ratios outside the accessible range of our models for some of their sample clusters (McLaughlin & van der Marel 2005 do not elaborate on this dependence). They found no significant correlation of M/L ratio with the distance of the cluster from the Galactic centre or the Galactic plane, in contrast to what might be expected from the BM03 simulations and our models (although the mixture of clusters with different masses at different Galactocentric radii, i.e., experiencing different tidal field strengths, could erase any correlation). However, the present-day cluster position within the Galaxy is probably less important to the total disruption time (and therefore the M/L ratio evolution) than the perigalactic distance and the number of past disk passages, which are unknown for most clusters. In addition, stochastic effects of the MF could induce additional scatter. The error bars are too large to enable us to identify a clear trend of M/L ratio with metallicity.

Of the 52 old clusters all but 8 are consistent within their 1σ ranges with models for [Fe/H] = –1.7 or [Fe/H] = –0.7. All of these 8 clusters have significantly too low M/L ratios. NGC 2419[5] and NGC 4590 both have metallicities[6] below [Fe/H] = –1.7, the lowest metallicity for which we can provide models. Those clusters could possibly be explained by models of even lower metallicity. For the other clusters (NGC 5272, NGC 5286, NGC 5904, NGC 6366, NGC 6715, NGC 7089), no immediate explanation (apart from underestimated observational uncertainties or the impact of the unknown perigalactic distance and past disk passages) is apparent. However, our new models represent a significant improvement: while 6 clusters are inconsistent with our new models, 21 clusters are inconsistent with the standard constant-M/L models.

Another way of analysing the properties of Milky Way globular clusters is shown in Fig. 8, where we compare their dereddened $V - I$ colours (taken from the Harris catalogue) with their M/L$_V$ ratios (as given by McLaughlin & van der Marel 2005). We overplot our models for a cluster age of 12 Gyr. The models with the longest disruption time are equivalent to the standard/non-dissolving model (marked with the red asterix). For decreasing disruption time, the models' M/L ratios drop,

[5] A re-analysis of the velocity dispersion of NGC 2419 by Baumgardt et al. (2009), indicates that the mass-to-light ratio is around 2, which is in good agreement with a canonical mass-to-light ratio and no dynamical cluster evolution.

[6] Data taken from the Harris catalogue Harris (1996), available at http://physwww.physics.mcmaster.ca/~harris/mwgc.dat

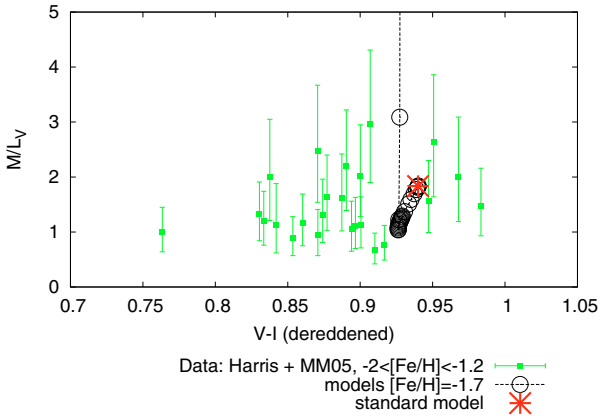

Fig. 8. Observations of old (∼12 Gyr) Milky Way globular clusters from the Harris catalogue (colours) and McLaughlin & van der Marel (2005) (M/L ratios). Shown is the relation between observed $V - I$ colour (dereddened) vs. M/L$_V$ ratio for metal-poor clusters.

before drastically increasing again at the final stages of dissolution. We restrict this analysis to metal-poor clusters ($-2 <$ [Fe/H] < -1.2), since the number of higher-metallicity clusters with the required data is too low to draw strong conclusions. We find good agreement between the observational data and our models for these clusters in terms of their M/L$_V$ ratios: the observational data are clearly spread over a wider range than the standard model could account for, while our new models cover this range in a far more comprehensive way. However, the observed cluster colours span a wide range in $V - I$ (although no colour uncertainties are available), which we cannot fully account for with our models. Our models might be about 0.05 mag too red for the observations. This could originate from our choice of isochrones (see Sect. 4.3, where we find that other isochrones infer results that are bluer than our set of isochrones). However, the other isochrones are then *bluer* than the observations, again by ∼0.05 mag. Other possible causes include uncertainties in the reddening estimates, and filter curve mismatch.

Data for massive star clusters in NGC 5128 (= Cen A) as well as massive objects (commonly referred to as "Ultra-Compact Dwarf galaxies" = UCDs) in the Virgo and Fornax galaxy cluster are taken from Mieske et al. (2008). These data include earlier observations by Rejkuba et al. (2007) for the star clusters in Cen A, and observations by a variety of authors for the UCDs (see Mieske et al. 2008, for details). While data for 27 of these clusters are not consistent with our new models, 47 clusters are not consistent with the standard constant-M/L models. Also for this sample, the new models provide significantly more accurate predictions.

We therefore conclude that the data of the samples are better described by our new models with preferential loss of low-mass stars, and we witness ongoing cluster dissolution. In future cluster modelling, this effect must clearly be taken into account.

Nonetheless, the sample of massive Cen A clusters and UCDs shows a very clear and strong trend of increasing M/L ratio with object mass, especially for metal-poor/intermediate metallicity objects (metal-rich objects are reasonably well covered by our models, except for the Virgo cluster UCD S490). This trend cannot be reproduced by our models: for masses higher than $\approx 10^7\ M_\odot$ only 3 out of 12 objects are consistent with our models within their respective 1σ uncertainties (one further object is marginally consistent). These massive systems are not expected to be mass-segregated because of their large relaxation time, let alone close to disruption (which in our models is the only possible way of reaching M/L ratios higher than predicted by standard stellar evolution). While the models do have inherent sources of uncertainties (e.g., the assumed initial-final mass relation for remnants, uncertainties in the underlying stellar isochrones, which will be studied in more detail in Sect. 4), they are unlikely to increase the model M/L ratios sufficiently to accommodate a significant fraction of the currently unexplained observations (especially without removing the agreement for objects of lower M/L ratios). Two possible explanations for the high M/L ratios would remain: either a stellar mass function that deviates significantly from the universal Kroupa (2001) IMF (see also Dabringhausen et al. 2008; Mieske & Kroupa 2008), or dark matter (see Baumgardt & Mieske 2008, for how dark matter can explain the high M/L ratios of UCDs).

3.3. Impact on age determination

Evolutionary synthesis models are regularly used to derive the physical parameters of star clusters (and galaxies) from observed spectrophotometry. The derived quantities are age, mass and metallicity of the star cluster as well as the extinction in front of the star cluster (see e.g., among many others, Bicker et al. 2002; Kassin et al. 2003; Anders et al. 2004b; de Grijs et al. 2004; Kundu et al. 2005; de Grijs & Anders 2006; Smith et al. 2007). Our GALEV models provide a model grid of SEDs as a function of age, metallicity, and dust extinction. The "AnalySED tool" (which we developed and tested in Anders et al. 2004a) compares these model SEDs with the observed SED of a star cluster using a χ^2 algorithm, to derive the best-fit model parameter combination and their respective uncertainty ranges from integrated multi-band cluster photometry.

We employ here the "AnalySED tool" to quantify the differences between the true ages of dissolving clusters (with a time-dependent MF) and the ages derived using the standard evolutionary synthesis models (with a MF fixed to the IMF slopes). We take the cluster photometry from the dissolving cluster models (for a number of filter combinations), apply Gaussian noise (with $\sigma = 0.1$ mag) to the photometry in the individual passbands, and analyse them using the standard, non-dissolving cluster models. The analysis is done for fixed solar metallicity and zero extinction, since leaving these parameters free to vary would lead to even stronger deviations from the standard models and larger uncertainties, as shown in Anders et al. (2004a). For each filter combination, total disruption time and age, we generate 1000 test clusters, derive their physical parameters, and determine the mean of the derived ages. The results in terms of the ratio of the derived mean age to the true cluster age are shown in Fig. 9.

For all models, the ages become overestimated for a significant fraction of the cluster lifetime (for some ages and models the ages can also be severely underestimated). This agrees well with the discussion concerning the cluster colours in Sect. 3.1: generally, when the cluster colours become redder than the standard models, the ages become overestimated. A direct comparison is not appropriate, however, because "AnalySED" uses the whole available spectral energy distribution (SED, i.e., the dataset containing all magnitudes in a given set of filters for a given cluster) to determine the model with the best-matching parameters, and hence differences in different filters can either cancel or amplify each other.

Datasets including the mid-UV (here represented by the ACS HRC *F220W* filter) show only modest deviations from the standard models (Fig. 9, top panels). However, 20% deviations are

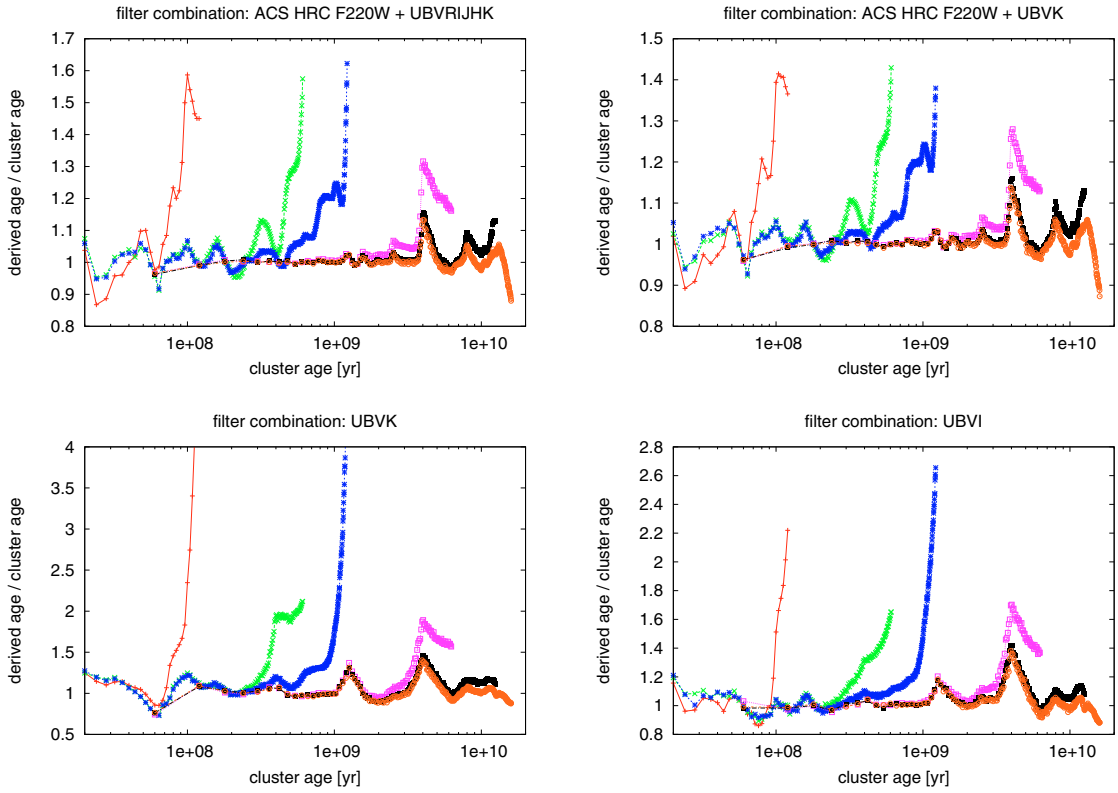

Fig. 9. Derived ages of dissolving star clusters with $t_{95\%}$ in the range 100 Myr–60 Gyr (*from left to right*: 100, 500 Myr, 1, 5, 10, 20 Gyr), using standard models, for a number of filter combinations. *Upper left panel*: ACS HRC *F220W* + standard *UBVRIJHK*, *top right*: ACS HRC *F220W* + standard *UBVK*, *bottom left*: standard *UBVK*, *bottom right*: standard *UBVI*. Shown is the ratio between the age derived using standard models and the age the dissolving cluster has.

regularly found. Datasets lacking the mid-UV, and especially those including near-IR data, are more sensitive to the changes in the mass functions (Fig. 9, bottom panels). For those datasets, deviations of 50% or even a factor ~2–3 are found.

4. Validation of the models

We investigate several uncertainties in our models, as well as comparing our new models with models previously released by our group. All the following values are *maximum* differences from the standard models of a given parameter in a given time interval, unless otherwise noted. In many cases the maximum deviations occur in the final stages of cluster dissolution, and for the longest total disruption times < maximum model age. If we had chosen a maximum model age of 13 Gyr instead of 16 Gyr, the maximum deviations would generally have been slightly smaller.

For the different issues discussed in this section, we also publish a few test cases on our webpage, illustrating the impact of different initial-final mass relations, isochrones, and parametrisations of the mass-function evolution on colours, masses, and mass-to-light ratios. For the parametrisations of the mass-function evolution, we select a few disruption times for presentation on our webpages, while for the initial-final mass relations and isochrones we present only data without disruption (i.e., pure stellar evolution) to avoid confusion.

4.1. Parametrisation of mass-function slope evolution

As discussed earlier, the mass-function slope evolution is derived from a subset of *N*-body simulations by BM03. The subset was selected to cover the parameter space well, while limiting the impact of low-number statistics (see Sect. 2.3).

The fit to the data of the time evolution of the mass function slopes is formally of very high accuracy because of the high number of data points. However, as shown in Figs. 2 and 3, the *N*-body models show an intrinsic spread around the fitted function. We quantified this spread to have a median value $\leq \pm 15\%$ for ages $\geq 1/3\ t_{95\%}$. For younger ages, this *relative* spread is larger, although the median of the *absolute* spread remains small, $\leq \pm 0.02$–0.03 change in the slope.

We test the impact of this spread by calculating models for which the time-dependent part of the mass function slope is reduced or increased by 15%. We find, as expected, that the change in the "high-mass slope" (i.e., for masses $\geq 0.3\ M_{\odot}$) is of primary importance, while the time-dependent contribution from stars with masses $\leq 0.3\ M_{\odot}$ changes the photometry only mildly. Since the mass evolutions of the cluster (total, luminous and remnant mass) were derived independent of the mass function evolution, the masses are not affected.

The impact of this uncertainty on the colors is small: the resulting changes for the models with the shortest disruption time $t_{95\%}$ (i.e., 100 Myr) and the colours with the longest wavelength coverage (i.e., $V-K$) reach ≈ 0.07 mag at final disruption. These changes decrease rapidly with increasing disruption time and decreasing wavelength coverage.

For ages $t \leq t_{95\%}$, the magnitudes change by ~0.15–0.2 mag (with the changes slightly larger for the shortest $t_{95\%}$ and red passbands). Since the mass is unaltered, this directly translates into a change in the M/L ratio by 15–20%.

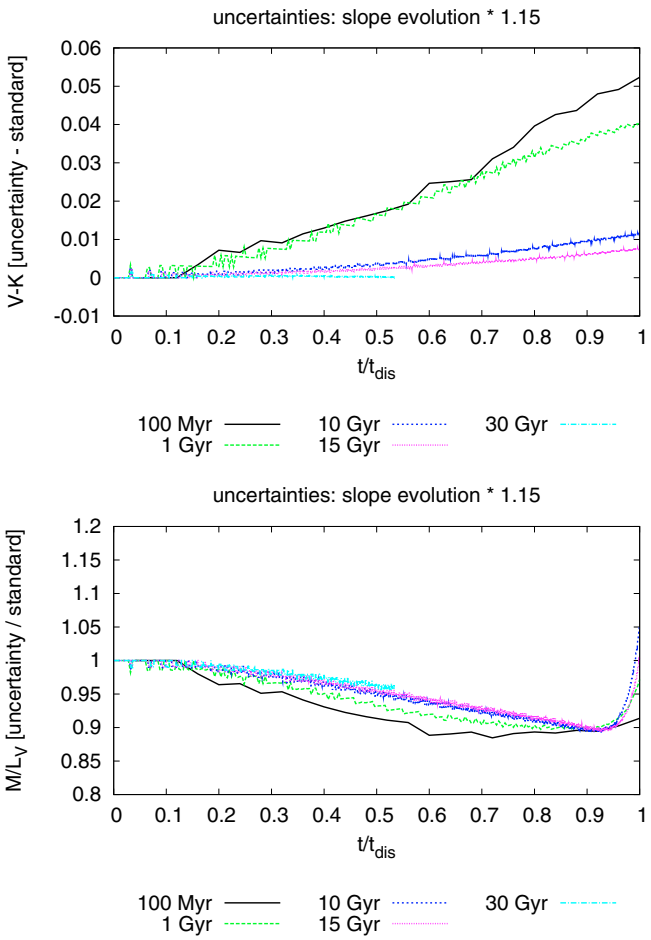

Fig. 10. Integrated $V-K$ colour (left panel) and M/L$_V$ ratio (*right panel*) for a Kroupa IMF, solar metallicity, our standard isochrones, a range of cluster disruption times, with the effect of MF evolution enhanced by 15% w.r.t. the standard models. Shown are the quantities relative to the respective quantities of our standard models. Diminishing the effect of MF evolution by 15% yields quantitatively similar results, however, the changes are in the opposite direction.

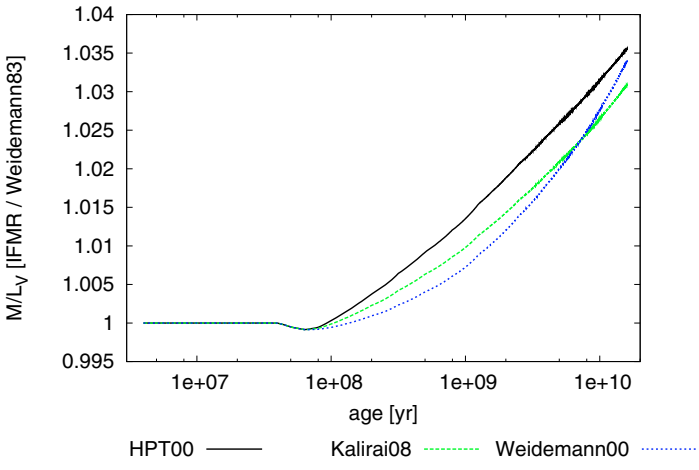

Fig. 11. M/L$_V$ ratio for a Kroupa IMF, solar metallicity, no cluster dissolution and the 3 alternative IFMRs discussed in the text. Shown are the quantities relative to the respective quantities of our standard models.

For ages $t > t_{95\%}$, both magnitudes and M/L ratios diverge from the models using the best-fit relation for the time evolution of the mass function slopes. Models with a weaker time evolution are increasingly brighter and have consequently lower M/L ratios.

In Fig. 10, we illustrate the effects of enhancing the MF evolution by 15%. Diminishing the effects of MF evolution by 15% provides quantitatively similar results, the changes with respect to the standard models being in the opposite direction. The $V-K$ colour evolutions represent the most extreme cases: effects become smaller for shorter wavelength coverage and longer disruption times.

In summary, the uncertainty induced by the spread in N-body model data around the fitted time evolution of the mass function slopes has an impact on the model predictions. However, for ages $t \leq t_{95\%}$ the induced uncertainties are much smaller than the error one makes by not taking into account the effect of preferential mass loss and cluster dissolution. In addition, we aim to describe the *average* cluster.

4.2. Initial-final mass relations

Our model results, especially the M/L ratios discussed in Sect. 3.2, depend on the treatment of stellar remnants. The remnant mass is calculated from the progenitor star's initial mass and the adopted initial-final mass relation (IFMR), which accounts both for mass loss during the life of the progenitor star and caused by the "death" of the star and remnant formation.

The IFMR for white dwarfs used in this work is based on the work by Weidemann & Koester (1983, hereafter "Weidemann83"). Since the IFMR remains uncertain, we tested our choice by adopting different IFMRs for white dwarfs, namely by Weidemann (2000, hereafter "Weidemann00"), by Kalirai et al. (2008) (hereafter "Kalirai08") and the prescription by Hurley et al. (2000, hereafter "HPT00"). For the latter one, we also adopted their IFMR for neutron stars, while for all other IFMRs we adopted Nomoto & Hashimoto (1988). Changes discussed below are given in relation to our standard IFMR Weidemann83.

We find the IFMR to be of minor influence on the results for ages $t \leq t_{95\%}$: the total mass changes by a maximum of 2–3%, while the luminous mass changes by 4% and 6% (for Weidemann00/Kalirai08 and HPT00, respectively). This translates into magnitude changes of ∼0.05 mag and ∼0.07 mag (for Weidemann00/Kalirai08 and HPT00, respectively). The associated effect on the M/L ratios is ∼4.5% and ∼6.5% (for Weidemann00/Kalirai08 and HPT00, respectively). For older ages $t \geq t_{95\%}$, the results eventually diverge. However, only in the last 5% of a cluster's lifetime do the total masses differ by more than 10%, regardless of the choice of IFMR. In Fig. 11, we show the impact of the chosen IFMR on the M/L$_V$ ratio for infinite disruption time.

4.3. Isochrones

Our choice of isochrones (i.e., isochrones from the Pavoda group, first presented in Bertelli et al. 1994 with later updates of the Padova group concerning the TP-AGB phase = "updated Padova94") is motivated by the following reasons:

1. to ensure consistency with GALEV models of galaxies, we require isochrones that cover the full mass range up to high

masses (ideally up to ∼120 $M_\odot$) to properly model ongoing star formation in galaxies;
2. likewise models covering a wide range in metallicities is desired to consistently model old/metal-poor globular clusters and young/metal-rich star clusters formed in nearby starbursts, as well as to model galaxies consistently from the onset of star formation to their present stage;
3. the models should cover all relevant evolutionary stages of these stars, especially the very luminous phases (for our study the TP-AGB phase especially is of prime importance, but early stages such as supergiants are also important).

It is regretable that recent high-quality isochrone calculations (e.g., Girardi et al. 2000; Yi et al. 2001; Cariulo et al. 2004; Pietrinferni et al. 2004, 2006; Bertelli et al. 2008) all focus on "low-mass" stars of maximum mass $\lesssim$10 $M_\odot$, although Bertelli et al. (2008) intend to present models up to 20 $M_\odot$ in the near future and/or do not fulfil one or more criteria mentioned above. However, stars more massive than $\approx$10 $M_\odot$ contribute significantly to the chemical enrichment and the light of young star clusters and most galaxies. The only models fulfilling all mentioned criteria are models by both the Padova group (Bertelli et al. 1994 plus TP-AGB updates) and by the Geneva group (Schaller et al. 1992; Charbonnel et al. 1993; Schaerer et al. 1993).

Since the main focus in this paper is systems older than ∼100 Myr we prefer the updated Padova94 isochrones over the Geneva isochrones. The alternative solution of combining isochrones from different groups/epochs, was rejected since consistency cannot be ensured.

We tested solar-metallicity isochrones by Cariulo et al. (2004), Pietrinferni et al. (2004), and Marigo et al. (2008) (also known as "Pisa/GIPSY", "BASTI", and "new Padova", respectively) with respect to the updated Padova94 isochrones used in this study, and derived star cluster models for test purposes. While the Pisa isochrones are offset from all other isochrones (they are generally significantly hotter, but are based on more limiting input physics), the other isochrones are in overall good agreement with the updated Padova94 isochrones. Small differences include:

- for increasing age, the BASTI main-sequence turn-off temperature goes from slightly cooler than the updated Padova94 to slightly hotter (by a few per cent). This results in an increasing deviation of U-/B-band magnitudes from the updated Padova94 isochrones by up to 0.5 mag. The new Padova isochrones show much smaller deviations $\lesssim$0.15 mag in these passbands. In contrast, for both BASTI and new Padova, colours such as $U-B$ or $B-V$ deviate for most of the time by $\lesssim$0.1 mag, and for the majority of time by $\lesssim$0.05 mag from the updated Padova94 models;
- overall, the RGBs and AGBs in the BASTI and new Padova isochrones are hotter than in the updated Padova94 isochrones. In particular, stars with the highest luminosities on the RGB/AGB are treated differently. For ages younger than ∼1 Gyr, the test models deviate significantly, both from our standard model as well as from each other. For ages $\gtrsim$2 Gyr, the BASTI and new Padova isochrones give comparable optical/NIR colours $V-I$ and $V-K$, but are offset from the updated Padova94 models by ∼–0.1 mag ($V-I$) and ∼–0.6 mag ($V-K$), in the sense that the updated Padova94 models are redder;
- the BASTI "non-canonical models" (i.e., with core convective overshooting during the H-burning phase) are closer to the updated Padova94 isochrones than their "canonical models" (i.e., without overshooting);
- the mass lost due to stellar evolution differs by between 2% (new Padova) and 7% (BASTI) from the updated Padova94 isochrones;
- the *relative* effects induced by the preferential mass loss (i.e., the difference between models with and without the effects of cluster dissolution) are qualitatively robust against the choice of isochrones. Small quantitative differences are present. However, they tend to be even stronger for the new isochrones than for the updated Padova94 isochrones.

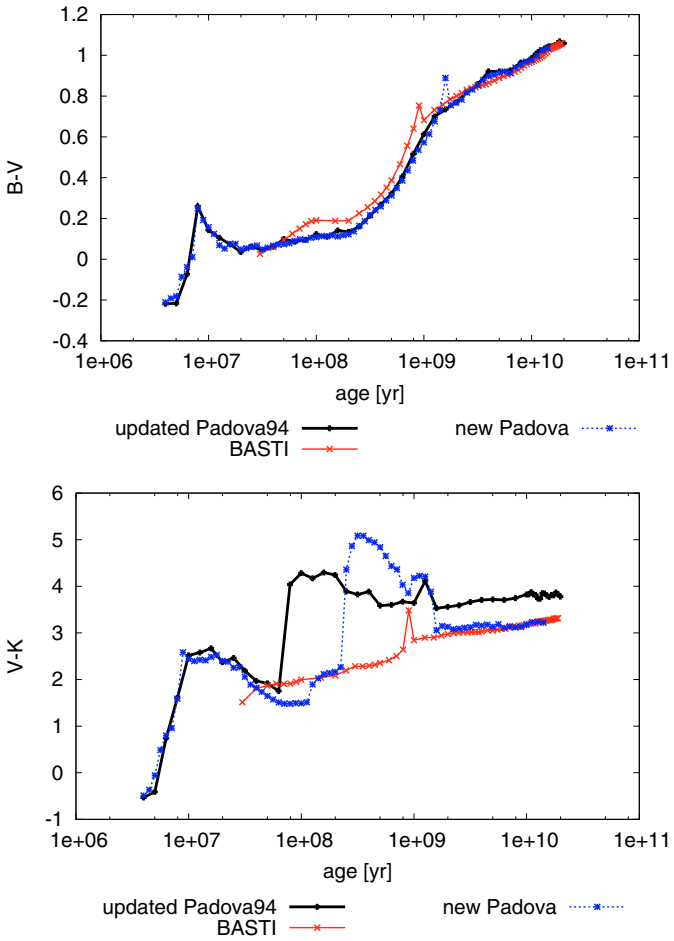

Fig. 12. Integrated $B-V$ (*left panel*) and $V-K$ colour (right panel) for a Kroupa IMF, solar metallicity, no cluster dissolution and 3 different sets of isochrones: the "upgraded Padova94" (our standard models, black lines), the "BASTI" isochrones (red lines, Pietrinferni et al. 2004) and the "new Padova" isochrones (blue dotted lines, Marigo et al. 2008).

For two example colours ($B-V$ and $V-K$), the time evolution for a standard SSP (i.e. without cluster dissolution) at solar metallicity is shown in Fig. 12. The blue colour $B-V$, dominated by hot stars mainly on the main sequence, shows good agreement between the investigated isochrones. The $V-K$ colour for ages younger than $\approx$1.5 Gyr is in strong disagreement between all three isochrones, up to 2.8 mag difference around an age of 300 Myr, showing strong differences in the treatment of the AGB phase. For older ages, the new Padova models agree well with the BASTI isochrones, but both are offset from the upgraded Padova94 by $\approx$0.6 mag.

To account for the uncertainty in the choice of isochrones, we plan to compile grids of dissolving cluster models, based on the BASTI, the new Padova and the Bertelli et al. (2008, once the extension to higher masses is published) isochrones, respectively, and release it on our webpage. These models will also employ the Kalirai et al. (2008) initial-final mass relation.

4.4. Comparison with earlier work

The new models presented here represent improvements to our earlier work (Lamers et al. 2006). In Lamers et al. (2006), we approximated the changes in the mass function by a time-dependent lower mass limit (i.e., assuming that only the lowest-mass stars are removed from the cluster, while higher-mass stars might only be removed by stellar evolution) and scaled our models to match the total mass in stars with $M < 2\ M_{\odot}$ with the BM03 simulations. This approach was improved by Kruijssen & Lamers (2008) by incorporating the effects of stellar remnants for clusters of different initial masses and different total disruption times for a range of metallicities. In that paper, the consequences of various physical effects on the photometry and M/L ratios were investigated, e.g., initial mass segregation, the role of white dwarfs and neutron stars, and the role of metallicity.

Because of the normalisation procedure, the *total* masses of the earlier models differs negligibly from the new models. However, the number of bright stars in the new models decreases more slowly with time than in the old models by Lamers et al. (2006) (the models by Kruijssen & Lamers 2008, represented already an improvement to earlier work, and are more consistent with the work presented here). Hence, the new models are brighter than the old models, especially for short disruption times. Consequently, the new mass-to-light ratio is lower, by 20–40%.

The new models are redder than the older ones, because the changing slope of the mass function slowly depopulates the (blue) main-sequence turn-off region already early on. In contrast, in the older models stars in the main-sequence turn-off region are removed more abruptly when the lower mass limit reaches the turn-off mass.

Before the lower mass limit reaches the turn-off mass in the old models, colours become slightly bluer for a short time, because almost all main sequence stars redder than the turn-off have been removed by then. This feature is not present in the new models, due to the more gradual mass loss. In addition, the old models show a strong reddening in their final stages, since the star cluster contains exclusively red giants/AGB stars (plus stellar remnants). This feature is also not strongly present in the new models, because the mass function, even close to total disruption, covers a wider range.

5. Conclusions

We have presented a novel suite of evolutionary synthesis models that accounts for the dynamical evolution of star clusters in a tidal field in a realistic manner. The dynamically induced changes in the stellar MF within the cluster and the overall mass loss of stars from the cluster into the surrounding field population is consistently taken into account[7].

Based on the simulations presented in BM03, we improved the parametrisation in the time evolution of the MF slope. We then combined this new description of the MF slopes with our *galev* evolutionary synthesis models. The resulting models, calculated for a range in metallicities and total cluster disruption times, were shown to deviate significantly from the canonical evolutionary synthesis models, which neglect the effects of dynamical cluster evolution. Depending on the total cluster disruption time and the colour index under investigation, differences of up to 0.7 mag (and in a large number of cases exceeding 0.1 mag) were found. These deviation were shown to lead to significant misinterpretations of the observations. For example, cluster age determinations can be wrong by 20–50%, or in extreme cases by up to a factor ~2–3. These deviations were found to depend strongly on the filter combination used to derive the ages: combinations including near-IR filters tend to be more sensitive to the changing MF, while for large wavelength coverage and/or large numbers of filters the deviations are still significant but generally smaller.

The M/L ratios are also strongly affected, and therefore so are photometric cluster masses derived from observations. For the largest part of a cluster's lifetime the M/L ratios are significantly below the canonical values (by up to a factor ~3–7). In late stages of cluster dissolution, the M/L ratios exceed the standard values, as the cluster mass becomes increasingly dominated by stellar remnants. This period can last for up to ~16% of the cluster's total disruption time. In both cases, the M/L ratios are strongly time-dependent. For fixed cluster age and/or fixed local disruption time, the dependence of M/L ratios on the presently observed cluster mass was investigated. They are broadly consistent with observations, although the observations show large scatter and uncertainties.

Our results confirm the trends in the evolution of colour and mass-to-light ratios of dissolving clusters, obtained by Kruijssen & Lamers (2008) and Kruijssen (2008), who used a simplified description of the changes in the mass function due to the preferential loss of low-mass stars in star clusters.

While the absolute values of our results depend on our choice of input physics, the general behaviour is robust against these choices. We will update our models whenever more sophisticated input physics becomes available.

Acknowledgements. P.A. acknowledges funding by NWO (grant 614.000.529) and the European Union (Marie Curie EIF grant MEIF-CT-2006-041108). P.A. and H.L. would like to thank the ISSI in Bern/Switzerland for their hospitality and support. P.A. would like to acknowledge fruitful discussions with Ines Brott and Rob Izzard, as well as with Diederik Kruijssen. Many thanks to Marina Rejkuba for a critical reading of the paper and asking the right questions. In addition, thanks to Marina Rejkuba and Steffen Mieske for kindly providing part of the observational data. P.A. is in Uta Fritzes debt for many years of teaching, advice and fruitful collaboration. This research was supported in part by the National Science Foundation under Grant No. PHY05-51164.

[7] The models are made publicly available on our webpages http://www.phys.uu.nl/~anders/data/SSP_varMF/ and http://data.galev.org for general use. They will also become available via CDS.

References

Anders, P., & Fritze-v. Alvensleben, U. 2003, A&A, 401, 1063
Anders, P., Bissantz, N., Fritze-v. Alvensleben, U., & de Grijs, R. 2004a, MNRAS, 347, 196
Anders, P., de Grijs, R., Fritze-v. Alvensleben, U., & Bissantz, N. 2004b, MNRAS, 347, 17
Bastian, N., & Goodwin, S. P. 2006, MNRAS, 369, L9
Baumgardt, H., & Makino, J. 2003, MNRAS, 340, 227
Baumgardt, H., & Mieske, S. 2008, MNRAS, 1255
Baumgardt, H., De Marchi, G., & Kroupa, P. 2008, ApJ, 685, 247
Baumgardt, H., Côté, P., Hilker, M., et al. 2009, MNRAS, 748
Bertelli, G., Bressan, A., Chiosi, C., Fagotto, F., & Nasi, E. 1994, A&AS, 106, 275
Bertelli, G., Girardi, L., Marigo, P., & Nasi, E. 2008, A&A, 484, 815
Bicker, J., Fritze-v. Alvensleben, U., & Fricke, K. J. 2002, A&A, 387, 412
Bicker, J., Fritze-v. Alvensleben, U., Möller, C. S., & Fricke, K. J. 2004, A&A, 413, 37

Boutloukos, S. G., & Lamers, H. J. G. L. M. 2003, MNRAS, 338, 717
Bruzual, G., & Charlot, S. 2003, MNRAS, 344, 1000
Cariulo, P., Degl'Innocenti, S., & Castellani, V. 2004, A&A, 421, 1121
Cerviño, M., & Mollá, M. 2002, A&A, 394, 525
Cerviño, M., & Luridiana, V. 2004, A&A, 413, 145
Cerviño, M., & Luridiana, V. 2006, A&A, 451, 475
Charbonnel, C., Meynet, G., Maeder, A., Schaller, G., & Schaerer, D. 1993, A&AS, 101, 415
Chen, L., de Grijs, R., & Zhao, J. L. 2007, AJ, 134, 1368
Dabringhausen, J., Hilker, M., & Kroupa, P. 2008, MNRAS, 386, 864
de Grijs, R., & Anders, P. 2006, MNRAS, 366, 295
de Grijs, R., Smith, L. J., Bunker, A., et al. 2004, MNRAS, 352, 263
Fagiolini, M., Raimondo, G., & Degl'Innocenti, S. 2007, A&A, 462, 107
Fioc, M. & Rocca-Volmerange, B. 1997, A&A, 326, 950
Gieles, M., & Baumgardt, H. 2008, MNRAS, 389, L28
Gieles, M., Bastian, N., Lamers, H. J. G. L. M., & Mout, J. N. 2005, A&A, 441, 949
Gieles, M., Portegies Zwart, S. F., Baumgardt, H., et al. 2006, MNRAS, 371, 793
Gieles, M., Athanassoula, E., & Portegies Zwart, S. F. 2007, MNRAS, 376, 809
Giersz, M., & Heggie, D. C. 1997, MNRAS, 286, 709
Gill, M., Trenti, M., Miller, M. C., van der Marel, R., Hamilton, D., & Stiavelli, M. 2008, ApJ, 686, 303
Girardi, L., Bressan, A., Bertelli, G., & Chiosi, C. 2000, A&AS, 141, 371
Goodwin, S. P., & Bastian, N. 2006, MNRAS, 373, 752
Gouliermis, D., Keller, S. C., Kontizas, M., Kontizas, E., & Bellas-Velidis, I. 2004, A&A, 416, 137
Harris, W. E. 1996, AJ, 112, 1487
Henon, M. 1969, A&A, 2, 151
Hurley, J. R., Pols, O. R., & Tout, C. A. 2000, MNRAS, 315, 543
Hurley, J. R., Tout, C. A., Aarseth, S. J., & Pols, O. R. 2004, MNRAS, 355, 1207
Kalirai, J. S., Hansen, B. M. S., Kelson, D. D., et al. 2008, ApJ, 676, 594
Kassin, S. A., Frogel, J. A., Pogge, R. W., Tiede, G. P., & Sellgren, K. 2003, AJ, 126, 1276
Kotulla, R., Fritze, U., Weilbacher, P., & Anders, P. 2009, MNRAS, 396, 462
Kroupa, P. 2001, MNRAS, 322, 231
Kruijssen, J. M. D. 2008, A&A, 486, L21
Kruijssen, J. M. D., & Lamers, H. J. G. L. M. 2008, A&A, 490, 151
Kundu, A., Zepf, S. E., Hempel, M., et al. 2005, ApJ, 634, L41
Küpper, A. H. W., Kroupa, P., & Baumgardt, H. 2008, MNRAS, 389, 889
Lada, C. J., & Lada, E. A. 2003, ARA&A, 41, 57
Lamers, H. J. G. L. M., Gieles, M., Bastian, N., et al. 2005a, A&A, 441, 117
Lamers, H. J. G. L. M., Gieles, M., & Portegies Zwart, S. F. 2005b, A&A, 429, 173
Lamers, H. J. G. L. M., Anders, P., & de Grijs, R. 2006, A&A, 452, 131
Larsen, S. S., & Richtler, T. 2004, A&A, 427, 495
Larsen, S. S., Brodie, J. P., & Hunter, D. A. 2004, AJ, 128, 2295
Leitherer, C., Schaerer, D., Goldader, J. D., et al. 1999, ApJS, 123, 3
Lejeune, T., Cuisinier, F., & Buser, R. 1997, A&AS, 125, 229
Lejeune, T., Cuisinier, F., & Buser, R. 1998, A&AS, 130, 65
Maccarone, T. J., & Servillat, M. 2008, MNRAS, 389, 379
Maraston, C. 2005, MNRAS, 362, 799
Marigo, P., Girardi, L., Bressan, A., et al. 2008, A&A, 482, 883
Marks, M., Kroupa, P., & Baumgardt, H. 2008, MNRAS, 386, 2047
McLaughlin, D. E., & van der Marel, R. P. 2005, ApJS, 161, 304
Mieske, S., & Kroupa, P. 2008, ApJ, 677, 276
Mieske, S., Hilker, M., Jordán, A., et al. 2008, A&A, 487, 921
Nomoto, K., & Hashimoto, M. 1988, Phys. Rep., 163, 13
Odenkirchen, M., Grebel, E. K., Dehnen, W., et al. 2003, AJ, 126, 2385
Pietrinferni, A., Cassisi, S., Salaris, M., & Castelli, F. 2004, ApJ, 612, 168
Pietrinferni, A., Cassisi, S., Salaris, M., & Castelli, F. 2006, ApJ, 642, 797
Pryor, C., & Meylan, G. 1993, in Structure and Dynamics of Globular Clusters, ed. S. G. Djorgovski, & G. Meylan, ASP Conf. Ser., 50, 357
Rejkuba, M., Dubath, P., Minniti, D., & Meylan, G. 2007, A&A, 469, 147
Salpeter, E. E. 1955, ApJ, 121, 161
Schaerer, D., Meynet, G., Maeder, A., & Schaller, G. 1993, A&AS, 98, 523
Schaller, G., Schaerer, D., Meynet, G., & Maeder, A. 1992, A&AS, 96, 269
Schulz, J., Fritze-v. Alvensleben, U., Möller, C. S., & Fricke, K. J. 2002, A&A, 392, 1
Smith, L. J., Bastian, N., Konstantopoulos, I. S., et al. 2007, ApJ, 667, L145
Spitzer, Jr., L., & Shull, J. M. 1975, ApJ, 201, 773
Tinsley, B. M. 1968, ApJ, 151, 547
Tinsley, B. M. 1980, Fund. Cosmic Phys., 5, 287
Tinsley, B. M., & Gunn, J. E. 1976, ApJ, 203, 52
Weidemann, V. 2000, A&A, 363, 647
Weidemann, V., & Koester, D. 1983, A&A, 121, 77
Worthey, G. 1994, ApJS, 95, 107
Yi, S., Demarque, P., Kim, Y.-C., et al. 2001, ApJS, 136, 417